Indian Journal of Pure & Applied Physics
Vol. 58, April 2020, pp. 298-303

Systematic study of nuclear structure properties of proton-rich even-even tellurium isotopes with the Gogny energy density functional

Shivali Sharma & Rani Devi*

Department of Physics, University of Jammu, Jammu 180 006, India

Received 17 February 2020

The ground state nuclear structure properties of the proton rich even-even tellurium isotopes are studied by using Gogny energy density functional within the framework of Hartree-Fock-Bogoliubov (HFB) method. The HFB equations are solved by using the axial cylindrical transformed deformed harmonic oscillator basis. The full parameterization of Gogny energy density functional is employed in the present study. The evolution of the neutron density distributions with an increase in neutron number is studied and emergence of various nuclear structure phenomena is investigated. Besides this, the ground state nuclear structure properties such as nuclear multipole moments, deformation parameters, binding energies, pairing energies, root mean square radii and charge radii are obtained for the even-even proton-rich tellurium isotopes. The theoretical results on the nuclear ground state properties are compared with the available experimental data and good agreement is found.

Keywords: Multipole moments, Root mean square radii, Hartree-Fock-Bogoliubov model, Transfomed harmonic oscillator basis

1 Introduction

Many experimental facilities are set up to produce nuclei close to the driplines, such as FAIR in GSI, Germany, RIBF at RIKEN, Japan, SPIRAL2 in GANIL, France, ISAC and ARIEL accelerators at TRIUMF, Canada. The structural properties of weakly bound nuclei near the driplines are a very challenging task for the existing theoretical models. The tellurium isotopes are an interesting set of nuclei with two proton particles away from the robust shell closure at proton number Z=50. The shape coexistence is also observed in the nuclei near Z=50 proton shell closure[1]. The lighter tellurium isotopes were supposed to be of vibrational character, but the comparable strengths of the $2_2^+ \rightarrow 2_1^+$ and $2_1^+ \rightarrow 0_1^+$ transitions in these isotopes and the systematic variation of the 0_2^+ energy levels gives one a hint that they might have transitional character. Another important feature of nucleus that play the key role in the study of nuclear structure is shape phase transition[2]. Also, many theoretical calculations have been carried out with several different frameworks[2-5] to study the shape transitions in nuclei. The variation of charge radii (r_c) along the isotopic mass chain gives the information about the nuclear matter behaviour. Now-a-days, theoretical framework based on the self-consistent mean field approaches with relativistic and non-relativistic interactions have achieved great success in describing the ground state bulk properties of nuclei[6-9]. The self-consistent mean field models based on different energy density functionals predict the various properties of nuclei like neutron radii for which few experimental data are available. Thus, layout of the neutrons inside a nucleus is at present only studied by theoretical predictions. However, the advancement in experimental facilities, viz elastic proton scattering[10] and coherent pion photoproduction from nuclei[11] and the advent of parity-violating elastic electron scattering facilities[12,13] have opened up new possibilities to determine the more precise value of neutron radii in near future. In the present paper, ground state bulk properties of proton-rich tellurium isotopes are studied within the framework of Hartree-Fock Bogiliubov (HFB) model with transformed harmonic oscillator (THO)[14] basis. The two-body finite range Gogny effective interactions are employed for the present study.

*Corresponding author (E-mail: rani_rakwal@yahoo.co.in)

2 Theoretical Framework

A brief description of the HFBTHO model is given here. For detailed description, see references[14-17]. A two-body Hamiltonian used to describe a system of fermions in HFB method can be expressed in a combination of annihilation and creation operators (c, c^+):

$$H = \sum_{n_1 n_2} e_{n_1 n_2} c^\dagger_{n_1} c_{n_2} + \frac{1}{4} \sum_{n_1 n_2 n_3 n_4} \bar{v}_{n_1 n_2 n_3 n_4} c^\dagger_{n_1} c^\dagger_{n_2} c_{n_4} c_{n_3} \quad \ldots (1)$$

where first term represents kinetic energy and $\bar{v}_{n_1 n_2 n_3 n_4} = \langle n_1 n_2 | V | n_3 n_4 - n_4 n_3 \rangle$ in the second term are anti-symmetrized two-body interaction matrix-elements. In HFB method, the quasiparticle vacuum $\alpha_k |\phi\rangle = 0$ represents ground state wave function $|\phi\rangle$. A linear Bogolyubov transformation is used to connect the quasiparticle operator (α, α^+) with the original particle operator as:

$$\alpha_k = \sum_n \left(U^*_{nk} c_n + V^*_{nk} c^\dagger_n\right),$$
$$\alpha^\dagger_k = \sum_n \left(V_{nk} c_n + U_{nk} c^\dagger_n\right) \quad \ldots (2)$$

It can be rewritten in matrix form as:

$$\begin{pmatrix} \alpha \\ \alpha^\dagger \end{pmatrix} = \begin{pmatrix} U^\dagger & V^\dagger \\ V^T & U^T \end{pmatrix} \begin{pmatrix} c \\ c^\dagger \end{pmatrix} \quad \ldots (3)$$

The matrices U and V satisfy the relations:

$$U^\dagger U + V^\dagger V = 1, \quad UU^\dagger + V^* V^T = 1,$$
$$U^T V + V^T U = 0, \quad UV^\dagger + V^* U^T = 0, \quad \ldots.(4)$$

In terms of normal density ρ and pairing tensor κ one-body matrices are defined as:

$$\rho_{nn'} = \langle \phi | c^\dagger_{n'} c_n | \phi \rangle = (V^* V^T)_{nn'},$$
$$\kappa_{nn'} = \langle \phi | c'_n c_n | \phi \rangle = (V^* U^T)_{nn'} \quad \ldots (5)$$

The expectation value of Hamiltonian (1) is expressed as an energy functional $E[\rho, \kappa] = \frac{\langle \phi | H | \phi \rangle}{\langle \phi | \phi \rangle}$

$$= \mathrm{Tr}\left[(e + \tfrac{1}{2}\Gamma)\rho\right] - \tfrac{1}{2}\mathrm{Tr}[\Delta \kappa^*] \quad \ldots (6)$$

Where

$$\Gamma_{n_1 n_3} = \sum_{n_2 n_4} \bar{v}_{n_1 n_2 n_3 n_4} \rho_{n_4 n_2},$$
$$\Delta_{n_1 n_2} = \frac{1}{2} \sum_{n_3 n_4} \bar{v}_{n_1 n_2 n_3 n_4} \kappa_{n_3 n_4} \quad \ldots (7)$$

The variation of $E[\rho, \kappa]$ with respect to normal density ρ and pairing tensor κ, results in HFB equations:

$$\begin{pmatrix} e + \Gamma - \lambda & \Delta \\ -\Delta^* & -(e + \Gamma)^* + \lambda \end{pmatrix} \begin{pmatrix} U \\ V \end{pmatrix} = E \begin{pmatrix} U \\ V \end{pmatrix} \quad \ldots (8)$$

where λ denotes Lagrangian multiplier and is used to fix the correct average particle number and Δ denotes pairing potential.It should be noted that the energy density functionals (6) have terms that cannot be simply related to particular effective interaction[17]. In terms of Gogny force, energy density functional can be derived from the two-body effective interaction[14,18]:

$$\hat{V}(\vec{r_1}, \vec{r_2}) = \sum_{j=1,2} e^{-(\vec{r_1} - \vec{r_2})^2 / \mu_j^2} \left(W_j + B_j \hat{P}_\sigma - H_j \hat{P}_\tau - M_j \hat{P}_\sigma \hat{P}_\tau\right) + t_0 \left(1 + \chi_0 \hat{P}_\sigma\right) \delta(\vec{r_1} - \vec{r_2}) \left[\rho^\alpha \left(\frac{\vec{r_1} + \vec{r_2}}{2}\right)\right] + iW_{LS} (\vec{\sigma}_1 + \sigma 2. \nabla 1 - \nabla 2 \times \delta r 1 - r 2 \nabla 1 - \nabla 2 \quad \ldots (9)$$

where $\hat{P}_\sigma$ and $\hat{P}_\tau$ are the spin and isospin operators. The first term in Eq. (9) is finite range term, consists of two Gaussian simulating a short and an intermediate range. All possible mixtures of spin and isospin operators denoted as P and are included in it. This term allows to treat the HF and pairing fields on the same footing without truncation of single-particle space. The second term represents a zero-range density-dependent part and the last term represents spin-orbit interaction. Equation (9) depends on 14 parameters and two finite ranges μ_1 and μ_2. The present calculations for proton-rich Te isotopes are performed by taking D1S, D1, D1p and D1N parameterizations of Gogny force. To save the computation time in case of Gogny interaction, the finite-range contributions to the HFB fields are computed in the configuration space. The following contractions of the matrix elements of the anti-symmetrized potential with density matrix ρ or pairing tensor κ are performed.

$$\Gamma_{n_1n_2} = \sum_{n_2n_4} \langle n_1 n_2 | \hat{V}\hat{A} | n_3 n_4 \rangle \rho_{n_4 n_2},$$

$$\Delta_{n_1n_2} = \frac{1}{2} \sum_{n_3n_4} \langle n_1 n_2 | \hat{V}\hat{A} | n_3 n_4 \rangle \kappa_{n_3 n_4} \quad \ldots (10)$$

3 Results and Discussion

The unconstrained axial deformed HFB+THO calculations[14] are performed for proton-rich Te isotopes taking D1S, D1, D1p and D1N parameterizations of Gogny force. The number of oscillator shells taken in the present calculation are 30. Both direct and exchange terms are included in the Coulomb interaction. For properly computing the level structure of Te nuclei, the local scale transformation of the single particle basis has been implemented. The calculated results with D1S parameterization show better agreement with the experimental data for binding energies, therefore, in this work the results obtained by taking D1S parameterization are presented for comparison with the experimental data.

3.1 Binding energy

The calculated binding energies are compared with the experimental data[19] in Fig. 1. From this figure, it is observed that both the experimental and calculated binding energies increase in magnitude in neutron number, thereby, showing that the stability of Te isotopes increases with an increase with neutron number. The absolute difference between the experimental and calculated values of binding energies is approximately 12 MeV.

3.2 Axial multipole moments

The axial multipole moments and deformation parameters obtained by D1S Gogny force are presented in Table 1. From this table, it is seen that the quadrupole (Q_2) moments show an increasing trend from N=54 to N=60, beyond N=60, the values of Q_2 show a decreasing trend with neutron number, there by indicating an increase in deformation from N=54-60 and a decrease in the degree of deformation as one moves from N=62-74 along the chain of Te isotopes. The present calculations predict the Te isotopes with N=54-60 as prolate deformed and N=62-74 as oblate deformed. The quadrupole deformation parameters (β_2) obtained in the present calculation are compared with the FRDM calculations[20] and the available experimental data[21].

3.3 Pairing energy

The calculated total pairing energy (E_p), is presented in Fig. 2. From this figure, it is seen that E_p shows a decreasing trend up to N=62. From N=62 to N=66, E_p increases as these Te isotopes lie in the mid shell region. Further, E_p decreases from N=66 to

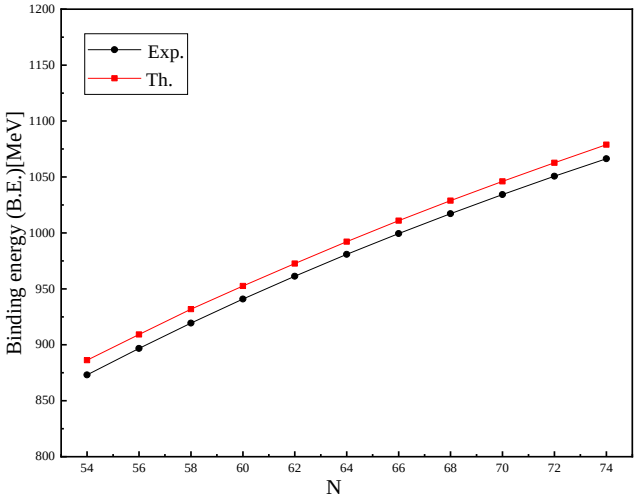

Fig.1 — Comparison of the experimental[19] and theoretical binding energies of $^{106\text{-}126}$Te isotopes.

Table 1 — Ground state properties of $^{106\text{-}126}$Te isotopes.

N	Quadrupole deformation parameter (β_2)			Quadrupole moment (b)	Hexadecupole moment (b^2)	Skin thickness (fm)
	Present calculation	FRDM[20]	Exp[21]			
54	0.16	0.119		4.308	0.268	-0.060
56	0.177	0.139		4.919	0.231	-0.037
58	0.189	0.150		5.426	0.221	-0.015
60	0.214	0.183		6.358	0.242	0.006
62	-0.165	0.194		-5.018	0.156	0.023
64	-0.167	0.216		-5.239	0.140	0.04
66	-0.167	-0.165		-5.376	0.121	0.057
68	-0.159	-0.176	0.201(21)	-5.251	0.094	0.074
70	-0.138	-0.166	0.1847(8)	-4.658	0.055	0.089
72	-0.118	-0.125	0.1695(9)	-4.101	0.021	0.103
74	-0.094	-0.094	0.1534(16)	-3.325	0.002	0.117

N=70 because of approaching the N=70 semi magic number. The peak at N=66 may be due to the precise mid shell position of ^{118}Te between closed shells N=50 to 82. The variation in pairing energy can be correlated to the change of deformation in Te isotopes with neutron number N (see table 1 and Fig. 2). Thus, the deformation in Tellurium isotopes increases as one moves from N=54-60, from N=62-68, it is almost constant and from N=68-74, again the deformation decreases. The prolate to oblate shape transition is predicted to take place as one moves from N=60-62.

3.4 Two neutron separation energy

The two-neutron separation energy (S_{2n}) is obtained from the binding energy (BE) by the expression:

$$S_{2n} = BE(Z,N) - BE(Z,N-2)$$

In Fig.3, the calculated S_{2n} is compared with the experimental data[19]. From this figure, it is seen that the calculated S_{2n} values are in agreement with the experimental data. The S_{2n} is maximum for N=56,58 and shows overall decreasing trend with neutron number.

3.5 Root mean square radii

In Fig. 4(a), the charge radii (r_c) are compared with the available experimental data[22]. The charge radius, r_c is computed by using the expression:

$$r_c = \sqrt{< r_p >^2 + < R_p^2 > + \frac{N}{Z} < R_n^2 > + \frac{3}{4M_p^2}}$$

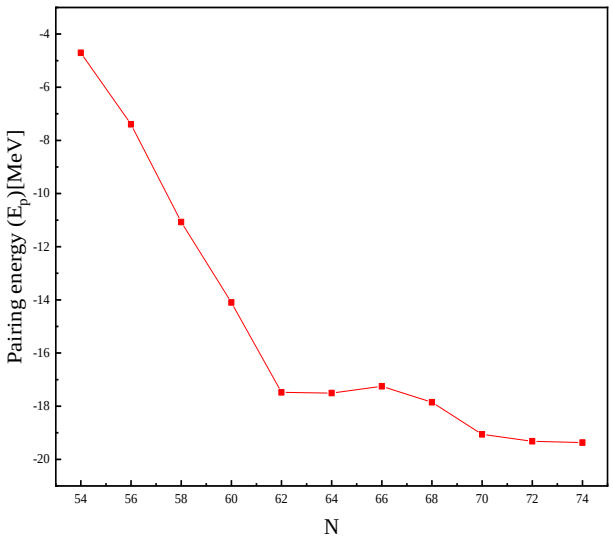

Fig. 2 — Pairing energy (E_p) as a function of neutron number (N).

where $< r_p >^2$ is the expectation value of the proton radius on the HFB vacuum; $< R_p^2 > (= 0.769\ fm^2)$ is the proton charge radius; $< R_n^2 > (= -0.1161\ fm^2)$ is the neutron charge radius and $\frac{3}{4M_p^2}(=0.033\ \ fm^2)$ is known as Darwin-Foldy term[23]. The calculated values of r_c, show a fairly good agreement with the available experimental data[22] (see Fig. 4(a)).

The calculated root mean square proton (r_p), neutron (r_n) and total (R_{rms}) radii are presented in Fig. 4(b). From this figure, it is seen that the r_p values with neutron number are nearly constant whereas r_n

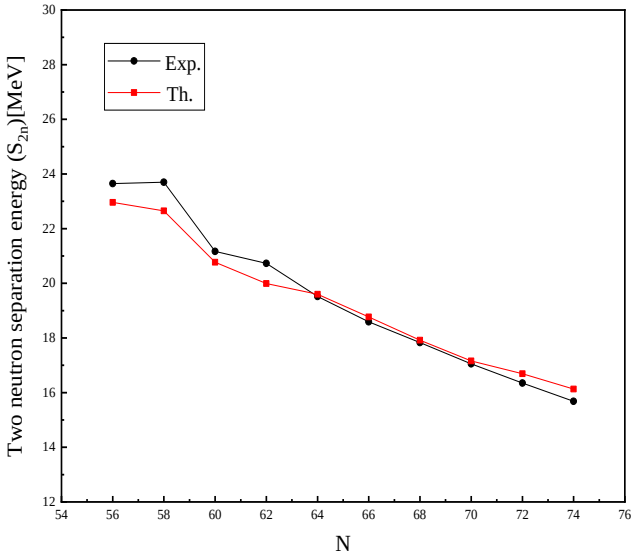

Fig. 3 — Comparison of experimental[19] and calculated two neutron separation energy (S_{2n}).

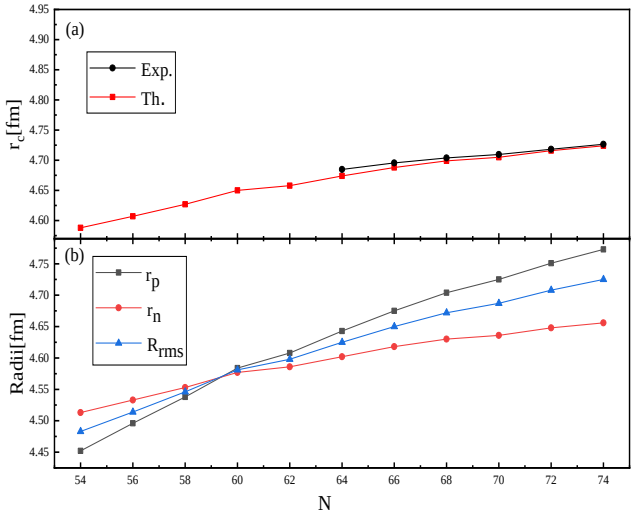

Fig. 4 — Comparison of experimental[22] and calculated charge radii (r_c) (a) and calculated neutron (r_n), proton (r_p) and root mean square radii (R_{rms}) (b).

values show an increase with neutron number. The r_n value changes from 4.452 for ^{106}Te to 4.773 for ^{126}Te. The difference between $(r_n-r_p)= \Delta r$, which is equal to skin thickness is also shown in Fig. 5. The skin thickness increases with increase in neutron number. The r_n values are less than r_p values from N=54 to 58, therefore Δr is negative (see also Table 1). From N=60 onwards, the r_n values are larger than that of the corresponding r_p values and hence, the values of ΔR become positive. The neutron density profiles of $^{106-126}$Te isotopes are plotted in Fig. 6. The figure shows that the spread of the neutron density distributions occur with an increase in neutron number. The major part of variation in the neutron density distributions are observed at the surface and tails with an increase in neutron number.

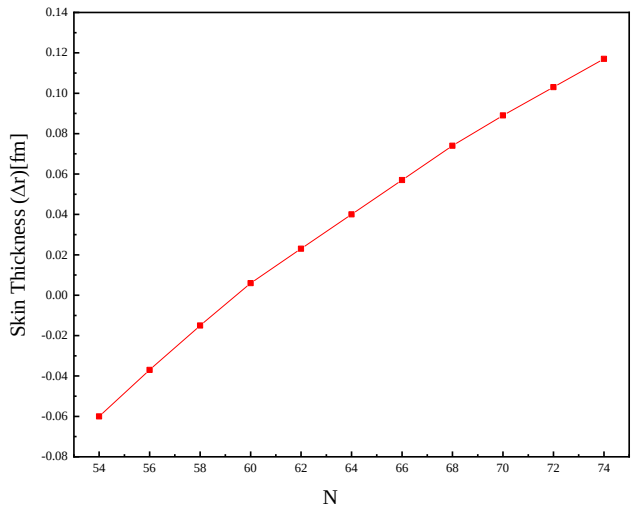

Fig. 5 — Variation of skin thickness (Δr) with neutron number (N).

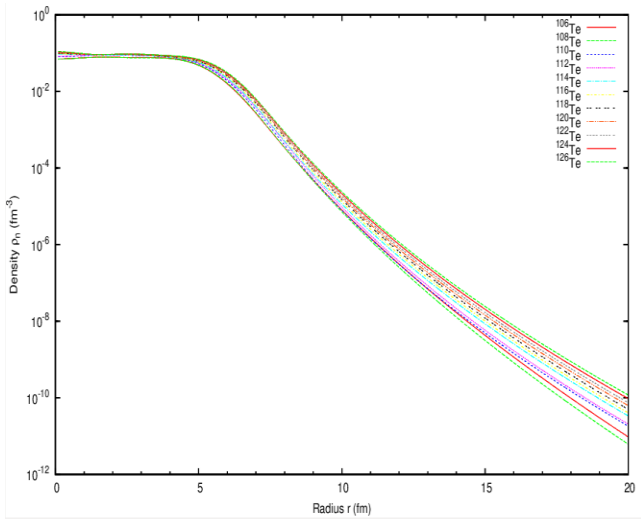

Fig. 6 — The variations in the neutron density distributions of $^{106-126}$Te.

4 Summary

The ground state properties of proton rich $^{106-126}$Te isotopesare studied in the HFB framework by using Gogny force. The available experimental data on mean square charge radii, skin thickness and quadrupole deformation are reproduced very well by the present calculations. The theoretical values for r_n are predicted for $^{106-126}$Te.Thus, the HFB framework with THO basis and Gogny D1S interaction, reproduces the ground state properties of proton-rich Te isotopes reasonably well.

Acknowledgement

One of the authors (SS) is grateful to Council of Scientific and Industrial Research, New Delhi for providing Junior research fellowship vide file no.:09/100(0227)/2019-EMR-1.

References

1 Wood J L, Heyde K, Nazarewicz W, Huyse M & Duppen P V, *Phys Rep*, 215 (1992) 101.
2 Cejnar P, Jolie J & Casten R F, *Rev Mod Phys*, 82 (2010) 2155.
3 Niksic T, Vretenar D, Lalazissis G A & Ring P, *Phys Rev Lett*, 99 (2007) 092502.
4 Li Z P, Niksic T, Vretenar D & Meng J, *Phys Rev C*, 81 (2010) 034316.
5 Shimizu N, Abe T, Honma M, Otsuka T, Togashi T, Tsunoda Y, Utsuno Y & Yoshida T, *Phys Scr*, 92 (2017) 063001.
6 Sharma S, Devi R & Khosa S K, *Nucl Phys A*, 988 (2019) 9.
7 Lalazissis G A, Niksic T, Vretenar D & Ring P, *Phys Rev C*, 71 (2005) 024312.
8 Niksic T, Vretenar D & Ring P, *Phys Rev C*, 78 (2008) 034318.
9 Bassem Y El & Oulne M, *Nucl Phys A*, 957 (2017) 22.
10 Zenihiro J, Sakaguchi H & Murakami T, *Phys Rev C*, 82 (2010) 044611.
11 Tarbert C M, Watts D P & Glazier D I, *Phys Rev Lett*, 112 (2014) 242502.
12 Abrahamyan S, Ahmed Z & Albataineh H, *Phys Rev Lett*, 108 (2012) 112502.
13 Horowitz C J, Kumar K S & Michaels R, *Eur Phys J A*, 50 (2014) 48.
14 Perez R Navarro, Schunck N, Lasseri R D, Zhang C & Sarich J, *Comput Phys Commun*, 220 (2017) 363.
15 Ring P & Schuck P, The Nuclear Many-Body Problem (Springer-Verlag, New York), 1980.
16 Dobaczewski J, Nazarewicz W, Werner T R, Berger J F, Chinn C R & Decharge J, *Phys Rev C*, 53 (1996) 2809.
17 Bender M, Heenen P H & Reinhard P G, *Rev Mod Phys*, 75 (2003) 121.

18 Decharge J & Gogny D, *Phys Rev C*, 21 (1980) 1568.
19 Wang M, Audi G, Kondev F G, Huang W J, Naimi S & Xing Xu, *Chin Phys C*, 41 (2017) 030003.
20 Moller P, Sierk A J, Ichikawa T & Sagawa H, *At Data Nucl Data Tables*, 109 (2016) 115.
21 Raman S, Nestor J C W & Tikkanen P, *At Data Nucl Data Tables*, 78 (2001) 1.
22 Angeli I & Marinova K P, *At Data Nucl Data Tables*, 99 (2013) 69.
23 Friar J L, Martorell J & Sprung D W L, *Phys Rev A*, 56 (1997) 4579.